X-622-66-335

NASA TM X-55560

THE INSTRUMENT FUNCTION OF A DIAGONAL-MOTION WIDE-ANGLE MICHELSON INTERFEROMETER SPECTROMETER

BY

WILLIAM D. JOHNSTON III

GPO PRICE $ _____

CFSTI PRICE(S) $ _____

Hard copy (HC) 2.00

Microfiche (MF) .50

JULY 1966

ff 653 July 65

GODDARD SPACE FLIGHT CENTER

GREENBELT, MARYLAND

X-622-66-335

THE INSTRUMENT FUNCTION OF A DIAGONAL-MOTION WIDE-ANGLE MICHELSON INTERFEROMETER SPECTROMETER

by

William D. Johnston III

July 1966

Goddard Space Flight Center
Greenbelt, Maryland

CONTENTS

THE INSTRUMENT FUNCTION OF A DIAGONAL-MOTION WIDE-ANGLE MICHELSON INTERFEROMETER SPECTROMETER

by

William D. Johnston III

SUMMARY

A wide-angle Michelson interferometer with a larger field of view, greater resolution and fewer reflecting interfaces than in the conventional instrument is described. A working model was made of glass half-cubes for visible light. An expression is derived for the instrument function and a plot shows its dependence on the field of view. The instrument can be used as an interferometer spectrometer for wavelengths ranging from the visible to the far infrared, particular attention being given here to the 5 to 30 micron range. Resolutions below one wave number seem feasible.

LIST OF SYMBOLS

Symbols	Quantity	Units (if any)
$\underset{\sim}{x}$	position vector	cm
λ	free space wavelength	cm
σ	wave number $= \frac{1}{\lambda}$	cm^{-1}
$n_{0,1,2}$, $n(\underset{\sim}{x})$, $n(\underset{\sim}{x}, \sigma)$	index of refraction, the subscripts refer to the thin gap, half-cube, and beam-splitter, respectively.	
$\hat{k}_i$, $\hat{k}(x)$	unit vector in direction of propagation of i^{th} wave, as a function of position if desired	–
$\hat{k}_{ix}$	x component of $\hat{k}_i$	–
$\underset{\sim}{k}(\underset{\sim}{x})$	wave vector $= \frac{2\pi}{\lambda} n(\underset{\sim}{x})\hat{k}$	cm^{-1}
ψ, $\psi(\delta, \theta)$, $\psi(\sigma, \delta, \theta)$	phase difference between beams in the two arms, as a function of variables desired emphasized	radians
α, β, γ	cosine angles of incident propagation vector	radians
θ, ϕ	colatitude and azimuth angles	radians
$\beta_M, \theta_M, \delta_M$	maximum values of variables	–
Ω	solid angle field of view $= \pi \theta_M^2$	steradians
δ, δ'	mirror position variables	cm
$h(\sigma, \delta)$	energy acceptance; or energy input to detector for unit spectral radiance per unit wave number interval, in watts	cm^2 steradians
$t_{0,2}$	thickness of beam splitter, thin gap	cm

LIST OF SYMBOLS (Continued)

Symbols	Quantity	Units (if any)
v	mirror velocity = δ_M / τ	cm/sec
ω	electronic signal frequency	radian/sec
A	aperture area	cm^2
τ	time of mirror motion = 2τ	sec
$\epsilon = \omega - s$	shifted frequency	radian/sec
$\delta(x)$	Dirac Delta function	inverse of x units
$Si(x)$	$= \int_0^x \frac{\sin y}{y}\, dy$	–
r	substitution for $\pi \sigma' v \theta_M^2 / n_i$	rad/sec
s	substitution for $4\pi n_1 \sigma' v(1 - \theta_M^2/4)$	rad/sec
$B(\sigma)$	Spectral radiance	watts/cm^2 – steradian cm^{-1}
$D_x(y)$	Rectangle function $= 1, \lvert y \rvert \leq x; = 0, \lvert y \rvert > x$	–
$T(\omega)$	electronic transfer function	–
$f(\sigma', \sigma)$	instrument function, or measured spectrum for monochromatic input with wavenumber σ'	$1/cm^{-1}$
Re [ ]	Operator taking real part of complex function	–
${}_tF_\omega\{f(t)\} \equiv \bar{f}(\omega)$	Fourier transform operator	sec
${}_\omega F_t^{-1}\{\bar{f}(\omega)\} = f(t)$	Inverse operator	radian/sec

THE INSTRUMENT FUNCTION OF A DIAGONAL-MOTION WIDE-ANGLE MICHELSON INTERFEROMETER SPECTROMETER

I. INTRODUCTION

In Fourier spectroscopy, as in other methods of spectroscopy, the field of view limits both the resolution and the energy acceptance of the instrument. Immersed interferometers make use of Snell's law to reduce the angle of incidence of a particular ray into the system, so that rays with incidence angles which are greater than some set maximum have refracted rays below this limit and can thus be included in the bundle of rays to be analyzed. Because of the mirror motion, it is generally easier to use a liquid as the immersing medium. The absorption bands of the liquid should not lie inside the portion of the spectrum of interest, the broadening of which severely limits the useable liquids.

When an electromagnetic wave crosses an interface between two media with different indices of refraction a certain amount of energy is reflected, the amount increasing with increasing difference in index of refraction. It is an advantage of the proposed configuration that the number of reflective interfaces is significantly reduced from that in the usual instrument.

An interferometer is described in which a novel diagonal motion of the mirror effectively achieves immersion with solid transmitting materials, an easily contained thin film of liquid being needed depending upon the index or refraction of the solid, the field of view, and the angle between the beam splitter and the mirror. The absorption and turbidity of the solid must then be considered. A model made of glass yielded fringes for both white light and the mercury green line.

Using the method of a previous report[2] the instrument function is found and plotted for several different values of field of view. The dependence on the maximum mirror displacement is discussed. Another interpretation of the plot yields information pertinent to optimum instrument design. As in the report[2] polarization effects are ignored and it is assumed that the beam splitter function does not depend on incidence angle or polarization state. The inclusion of these effects is straightforward but lengthy, and would alter the results only to a very small extent.

II. THE PROPOSED CONFIGURATION

A. Physical Description

The proposed configuration is shown in cross-sectional view in Figure 1. Its construction might proceed as follows: a cube of material with low turbidity

and good transmission in the range of interest is laid flat and cut vertically along a diagonal. The diagonal faces are polished and a high index of refraction layer of non-absorbing material is evaporated onto one face to serve as a beam splitter. The cube faces indicated by g, are coated to serve as plane reflecting mirrors. Instead of having a flat surface at j, an off-axis parabolic surface is ground and coated to act as a mirror lens to focus the radiation onto the detector which is mounted in the focal plane of the parabola. The two pieces are then supported so that the small gap is maintained constant during the relative motion parallel to the diagonal faces, as indicated by the arrows. As will be discussed, optical reasons might demand filling the gap with a fluid to avoid total internal reflection at the interface ℓ.

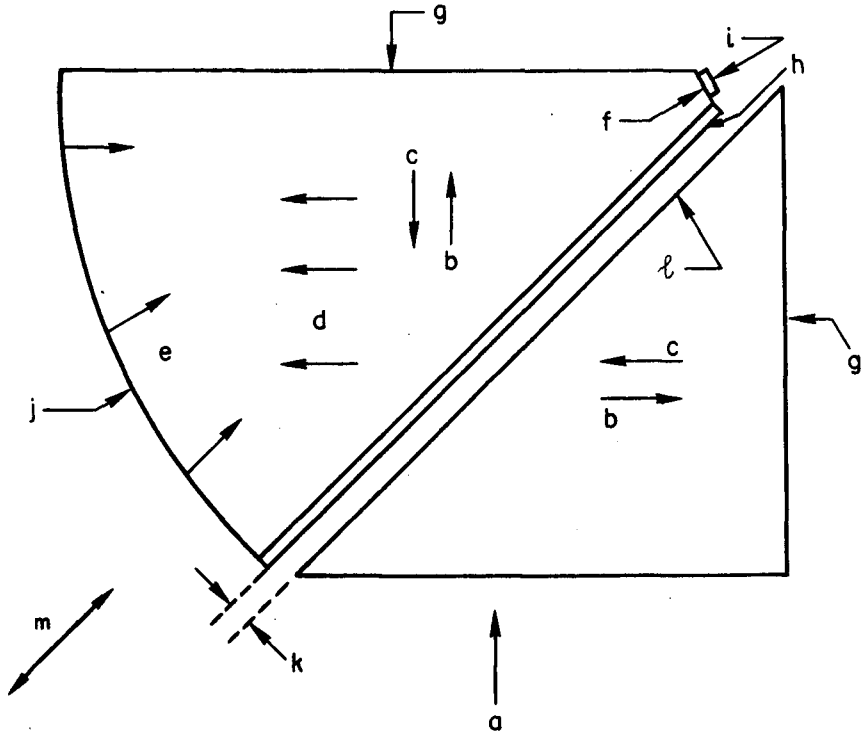

a. Radiation incident on instrument and
b. amplitude divided by beam splitter into two beams,
c. reflected by mirrors of each arm to interfere and form
d. composite beam which is
e. focused by parabola
f. onto the detector.
g. Plane mirror surfaces
h. Beam splitter
i. Detector
j. Parabolic mirror surface
k. Thin gap, perhaps filled with liquid.
l. Interface of potential total internal reflection.
m. Line of relative motion.

Figure 1–The Proposed Configuration

Figure 2 shows how the proposed configuration has approximately 50% fewer reflective interfaces than does the usual instrument. Each arrow represents an undesired reflection at an interface by a wave, the composite wave being regarded as only one wave, and the round headed arrows indicating an undesired reflection in the conventional configuration which is eliminated in the proposed configuration. The ratio of undesirable crossings is 8 to 15.

Various configurations for collecting the energy of the composite beam are possible. If the detector can be mounted in optical contact with the material then there is only one reflecting interface to be crossed before the radiation is absorbed and converted to a signal. Or it might be advantageous to grind a lens surface on the material, as in Figure 3.

A simple model of the proposed instrument was made from available glass half-cubes coated with aluminum to form the mirrors and the beamsplitter, a film of 40 angstrom units corresponding to approximately 50% reflectivity. Figure 4a shows the half-cubes and 4b shows the fringes obtained with the mercury green line. White light fringes were also obtained; their visibility of course decreased rapidly with increase in fringe order. The gap between the diagonal faces was filled with light lubricating oil to prevent total internal reflection. This provided lubrication and allowed a smooth mirror motion. The fringe patterns did not appear overly sensitive to the thickness of this gap, and the relative motion was very smooth.

B. Mathematical Description

A derivation of the energy input to the detector as a function of incident radiation, mirror position, and field of view is now given using the method discussed in a previous report.[2] The analysis is based on the instrument of Figure 5, the coordinate system indicated being right-handed with the z-axis coming out of the paper. The arrows indicate the propagation directions of the plane wave in the different parts of the instrument.

The phase difference between the two beams which recombine to form the composite wave which transports energy to the detector is given by

$$\psi = \oint_{\text{x arm}} \underset{\sim}{k}(\underset{\sim}{x}) \cdot d\underset{\sim}{x} - \oint_{\text{y arm}} \underset{\sim}{k}(\underset{\sim}{x}) \cdot d\underset{\sim}{x}$$

where $\oint_{\text{x arm}}$ denotes a closed line integral along the path a-b-c-b-a, $\oint_{\text{y arm}}$ corresponds to a-d-e-d-a and where the appropriate wave vector $\underset{\sim}{k}(\underset{\sim}{x}) = n(\underset{\sim}{x})\, 2\pi/\lambda\, \hat{k}(\underset{\sim}{x})$ must be chosen for each part of the path. Thus the difference in optical length between the two paths is

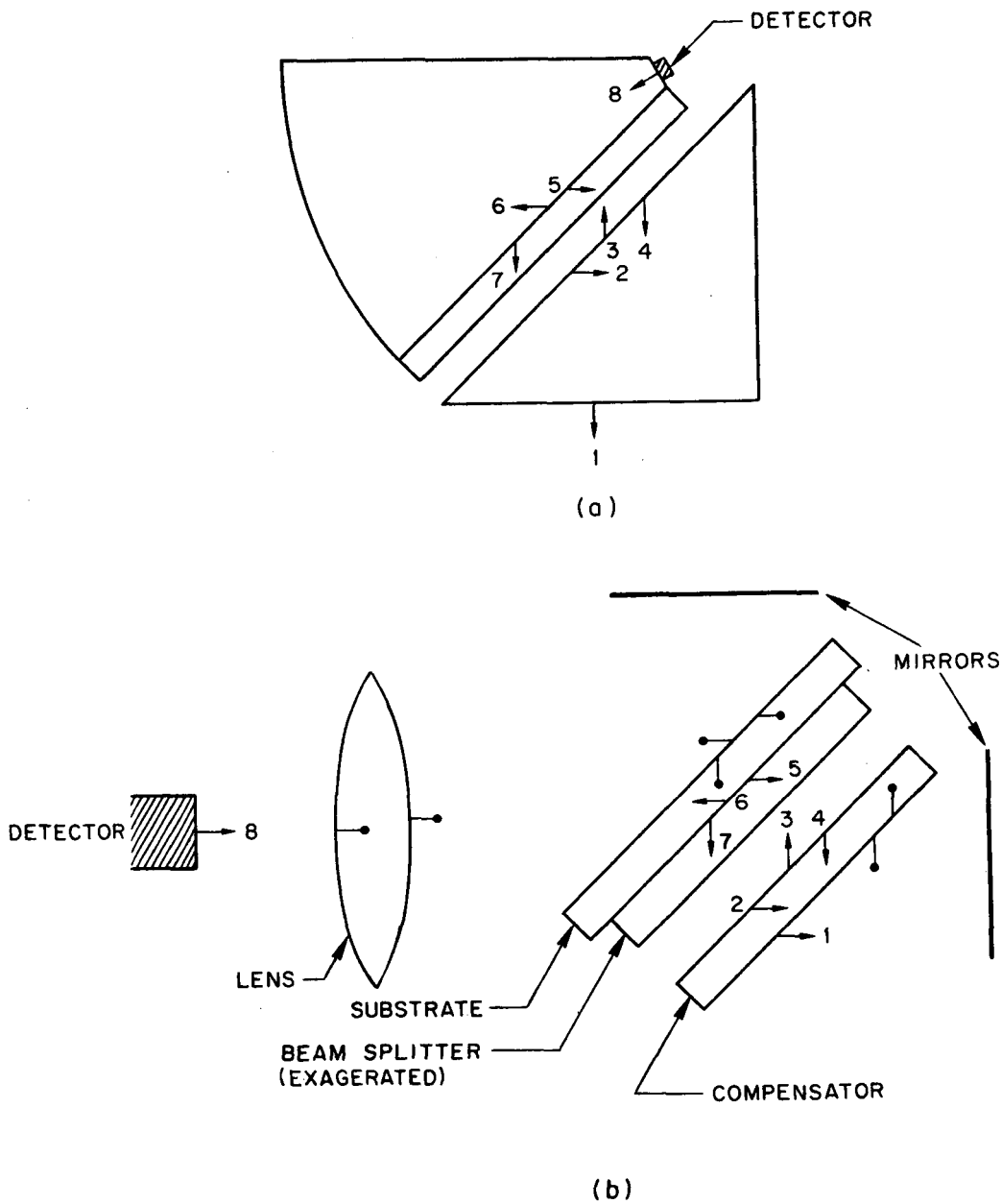

Figure 2–Comparison of the number of reflective interfaces in the (a) proposed and (b) conventional configurations. The numbers indicate corresponding reflections in the two cases. The round-headed arrows indicate reflections in the conventional instrument which do not occur in the proposed configuration.

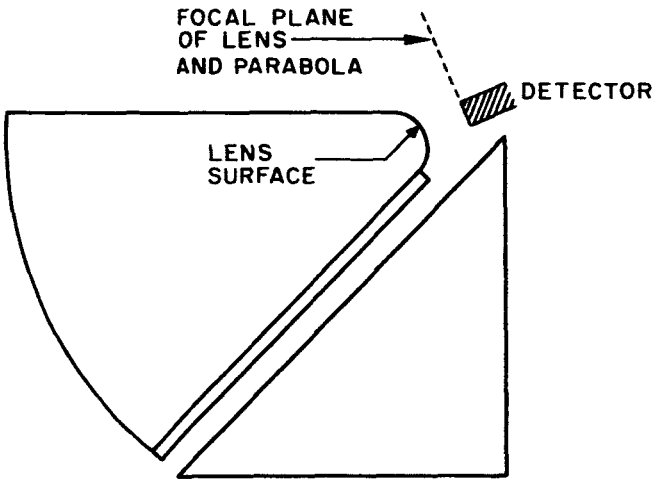

(a)

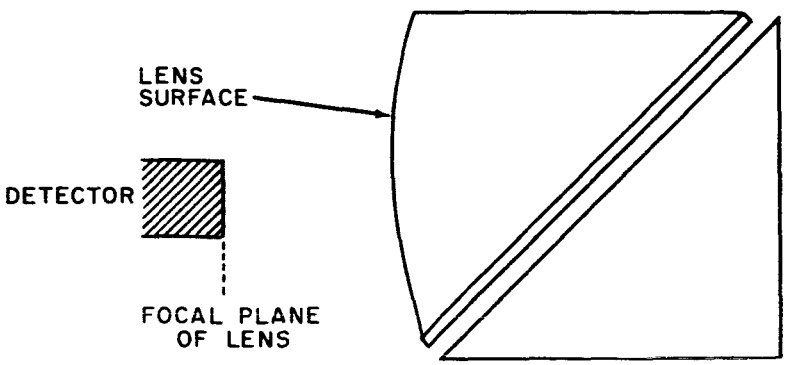

(b)

Figure 3–Lens surfaces on cube. (a) To allow for smaller area detector, and (b) Lens alternative to parabolic mirror.

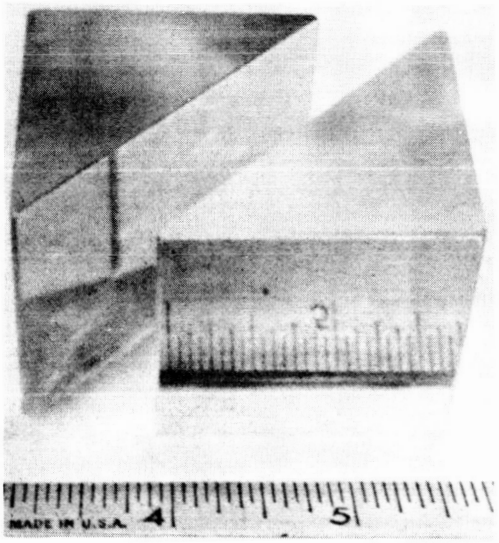

(a) Glass half-cubes used for working model of proposed interferometer. The somewhat damaged beamsplitter is on the diagonal face shown.

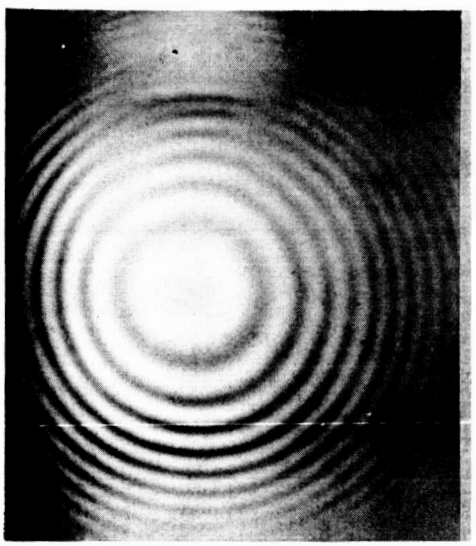

(b) Fringes obtained with mercury green line

Figure 4

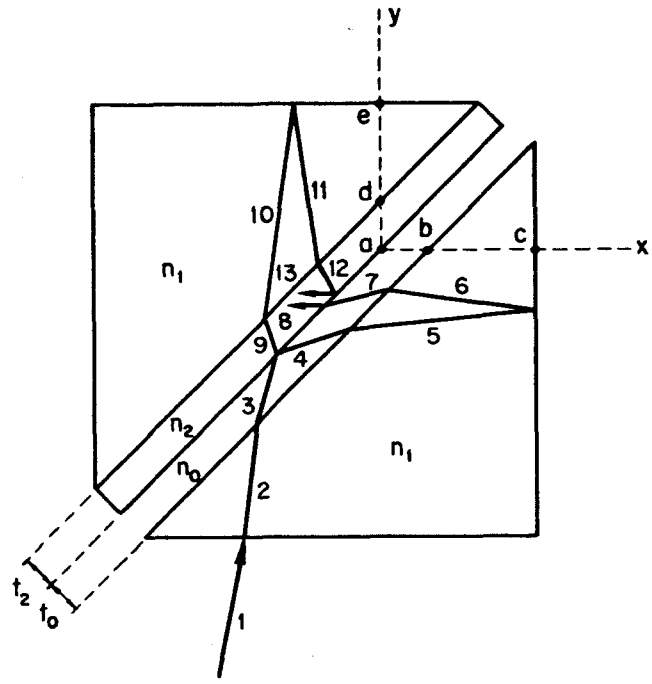

Figure 5–Propagation of plane wave in arms of proposed configuration.

$$\frac{\lambda}{2\pi}\psi = \sqrt{2}\, t_0\, n_0\, (\hat{k}_{4x} - \hat{k}_{7x}) + \left(\delta + \frac{a}{2}\right) n_1\, (\hat{k}_{5x} - \hat{k}_{6x}) - \sqrt{2}\, t_2\, n_2\, (\hat{k}_{9y} - \hat{k}_{12y})$$

$$- \frac{a}{2} n_1\, (\hat{k}_{10y} - \hat{k}_{11y})$$

where motion of the bottom half-cube along the diagonal by an amount $\sqrt{2}\,\delta$ cm results in a mirror motion of δ cm. The reported method explains how to find all the $\hat{k}_i$ as a function of any given incident unit vector

$$\hat{k}_1 = [\cos\alpha,\ \cos\beta,\ \cos\gamma],$$

and the unit vectors normal to the interfaces and mirrors. The cosine angles are as shown in Figure 6.

By use of the definitions

$$A = \sqrt{n_1^2 - \sin^2 \beta}, \qquad B(\pm) = \frac{1}{2}(\cos \alpha \pm A)$$

$$C(i, \pm) = \frac{1}{\sqrt{2}} \sqrt{n_i^2 - n_1^2 + 2B^2 (\pm)}$$

the unit propagation vectors are:

$$\hat{k}_2 = \frac{1}{n_1} [\cos \alpha, A, \cos \gamma]$$

$$\hat{k}_3 = \frac{1}{n_0} [B(+) - C(0, -), B(+) + C(0, -), \cos \gamma]$$

$$\hat{k}_4 = \frac{1}{n_0} [B(+) + C(0, -), B(+) - C(0, -), \cos \gamma]$$

$$\hat{k}_5 = \frac{1}{n_1} [A, \cos \alpha, \cos \gamma]$$

$$\hat{k}_6 = \frac{1}{n_1} [-A, \cos \alpha, \cos \gamma]$$

$$\hat{k}_7 = \frac{1}{n_0} [B(-) - C(0, +), B(-) + C(0, +), \cos \gamma]$$

$$\hat{k}_9 = \frac{1}{n_2} [B(+) - C(2, -), B(+) + C(2, -), \cos \gamma]$$

$$\hat{k}_{10} = \hat{k}_2$$

$$\hat{k}_{11} = \frac{1}{n_1} [\cos \alpha, -A, \cos \gamma]$$

$$\hat{k}_{12} = \frac{1}{n_2} [B(-) + C(2, +), B(-) - C(2, +), \cos \gamma]$$

Thus

$$\frac{\lambda}{2\pi}\psi = 2\delta\sqrt{n_1^2 - \sin^2\beta} + t_0\left[\sqrt{2}\sqrt{n_1^2 - \sin^2\beta} + \sqrt{n_0^2 - n_1^2 + \frac{1}{2}\left(\cos\alpha + \sqrt{n_1^2 - \sin^2\beta}\right)^2}\right.$$

$$\left. + \sqrt{n_0^2 - n_1^2 + \frac{1}{2}\left(\cos\alpha - \sqrt{n_1^2 - \sin^2\beta}\right)^2}\right]$$

$$- t_2\left[\sqrt{2}\sqrt{n_1^2 - \sin^2\beta} + \sqrt{n_2^2 - n_1^2 + \frac{1}{2}\left(\cos\alpha + \sqrt{n_1^2 - \sin^2\beta}\right)^2}\right.$$

$$\left. + \sqrt{n_2^2 - n_1^2 + \frac{1}{2}\left(\cos\alpha - \sqrt{n_1^2 - \sin^2\beta}\right)^2}\right]$$

where t_0 and t_2 are thicknesses of the gap and beam splitter coating

Figure 6 indicates a more useful coordinate system related to the cosine angles by $\beta = \theta$

$$\cos\alpha = \sin\theta\cos\phi$$
$$\cos\gamma = -\sin\theta\sin\phi$$

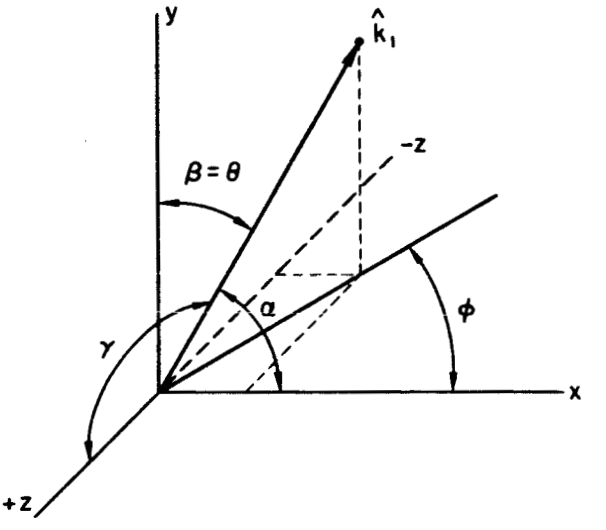

Figure 6

Replacement of α and β yields

$$\frac{\lambda}{2\pi}\psi = 2\delta\sqrt{n_1^2 - \sin^2\theta} + t_0\left[\sqrt{2}\sqrt{n_1^2 - \sin^2\theta}\right.$$

$$\left. + \sqrt{n_0^2 - n_1^2 + \frac{1}{2}\left(\sin\theta\cos\phi + \sqrt{n_1^2 - \sin^2\theta}\right)^2} + \sqrt{n_0^2 - n_1^2 + \frac{1}{2}(\sin\theta\cos\phi - \sqrt{\ldots})^2}\right]$$

$$- t_2\left[\sqrt{2}\sqrt{n_1^2 - \sin^2\theta} + \sqrt{n_2^2 - n_1^2 + \frac{1}{2}\left(\sin\theta\cos\phi + \sqrt{n_1^2 - \sin^2\theta}\right)^2}\right.$$

$$\left. + \sqrt{n_2^2 - n_1^2 + \frac{1}{2}(\sin\theta\cos\phi - \sqrt{\ldots})^2}\right]$$

The angle ϕ varies from zero to 2π but θ varies in the range of a few degrees about zero and thus an expansion to 4th order is useful. The factor of t_0 then becomes equal to

$$\sqrt{2}\,n_1\left[1 - \frac{\theta^2}{2n_1^2} + \theta^4\left(\frac{1}{6n_1^2} - \frac{1}{8n_1^4}\right)\right] + 2\sqrt{n_0^2 - \frac{n_1^2}{2}}\;\left[1 + \theta^2 A + \theta^4 B\right],$$

with

$$A = \frac{-\sin^2\phi}{2n_0^2 - n_1^2} - \frac{n_1^2\cos^2\phi}{2n_0^2 - n_1^2} < 1$$

$$B = \frac{\sin^2\phi}{3(2n_0^2 - n_1^2)} - \frac{\sin^4\phi - 2n_1^2\cos^2\phi\left(\frac{1}{3} - \frac{1}{n_1^2}\right)}{4(2n_0^2 - n_1^2)}$$

The t_2 factor is the same with n_2 replacing n_0. It is then possible to adjust the parameters t_0, t_2 n_0 n_2 so that the coefficient of the θ^2 term equals zero [or better yet so that θ^2 (. . .) + θ^4 (. . .) is a minimum at θ_{max}. The coefficient of the θ^4 term has less than unity order of magnitude. For a maximum $\theta = 10° \times \pi/180 = .175$, $\theta^2 = .030$, and $\theta^4 = .001$.

The angular dependence of ψ on the coefficients of t_0, t_2 is such that it is multiplied by θ^2, or θ^4 and since the overall θ^2 term can be made to vanish, the angular dependence, itself of the order of unity, is reduced by $\theta^4 = 10^{-3}$.

Thus the t_2 and t_0 terms have angular dependence only in the terms multiplied by θ^2 and θ^4 and the θ^2 term can be made to vanish by certain choices at the parameters. The conclusion is then that they may be completely neglected, since the zero order term is a small constant which is multiplied by the few microns thicknesses t_2, t_0 ; and the overall effect is then a small constant contribution to the phase difference. Thus the beamsplitter and thin gap can be several wavelengths thick; the effect on the interferogram being a slight dispersion.

Thus the optical path difference is

$$\frac{\lambda}{2\pi}\psi = 2\delta\sqrt{n_1^2 - \sin^2\theta} = 2\delta n_1\left[1 - \frac{\theta^2}{2n_1^2} + \theta^4\left(\frac{1}{6n_1^2} - \frac{1}{8n_1^4}\right)\right] \qquad (1)$$

which depends only on the mirror position and the angle measuring how far off – axis is the incident plane wave. The flux of energy into the detector due to a plane wave incident at θ is proportional to [A cos θ] [cos (ψ)] [2π sin θ d θ] where the first bracket is the aperture area and the third is the differential solid angle. Integration of θ yields the energy input to the detector, assuming unit spectral radiance, per unit wavenumber interval centered on σ:

$$h(\sigma, \delta) = \int_0^{\theta_m} A\left(1 - \frac{\theta^2}{2}\right)\cos\left\{4\pi\sigma n_1\delta\left[1 - \frac{\theta^2}{2n_1^2} + \theta^4\left(\frac{1}{6n_1^2} - \frac{1}{8n_1^4}\right)\right]\right\} 2\pi\left(\theta - \frac{\theta^3}{6}\right)d\theta$$

Evaluation of the integral, neglecting higher than second order terms in θ, leads to the form commonly seen in the literature,[4] except for the appearance of n_1:

$$h(\sigma, \delta) = \frac{n_1 A}{\sigma \delta} \sin \frac{\pi \sigma \delta \theta_M^2}{n_1} \cos \left[4\pi \sigma \delta n_1 \left(1 - \frac{\theta_M^2}{4 n_1^2} \right) \right] \qquad (2)$$

The evaluation of the integral, however, is not necessary in evaluating the usefulness of the proposed instrument. The important consideration is that the phase difference is a function of not only mirror position and wave number but also of incidence angle θ: $\psi(\sigma, \delta, \theta)$. Thus, in general, at any given mirror position, the phase condition varies with θ, and it is the cosine of this quantity which determines the input of radiant energy into the detector. Field compensation denotes a minimizing of this dependence and thus this instrument has perfect field compensation at the mirror position $\delta = 0$, and the worst compensation at the largest value of δ. As shown in an approximate treatment in ref. 2, the detector output is reduced to zero when

$$\psi(\sigma, \delta, 0) - \psi(\sigma, \delta, \theta_M) = 2\pi,$$

where it is assumed that the incident radiation is homogeneous in direction and completely fills the circular field of view. We then take this to be our criterion to define the maximum allowable mirror motion $\delta_M(\sigma, \theta_M)$ as a function of wave number and maximum half-angle of the conical field of view. Thus from

$$-2\pi = 4\pi \sigma \delta_M n_1 \left[-\frac{\theta_M^2}{2 n_1^2} + \theta_M^4 \left(\frac{1}{6 n_1^2} - \frac{1}{8 n_1^4} \right) \right]$$

relating the limits on mirror motion and field of view. For θ_M below $10° = .001$ rad the θ^4 term can be neglected, leaving, for $\sigma = 2000\ \text{cm}^{-1} = 1/5\,\mu$

$$1 = \frac{2000}{n_1} \delta_M \theta_M^2 . \qquad (3)$$

The field of view is $\Omega = \pi \theta_M^2$ and thus field of view and index of refraction are linearly related, and to increase the first by a certain factor, the second must be increased by the same factor. If a mirror motion about $\delta = 0$ of .1 cm is considered then $\delta_M = \pm .1$ and

$$1 = \frac{2000\,(.1)}{n_1}\,\theta_M^2, \qquad \theta_M = 4.15\,\sqrt{n_1}\ \text{degrees}$$

since $\sqrt{1.5} = 1.225$, $\sqrt{2} = 1.41$ it becomes obvious how the immersion allows an increased field of view. This motion yields a maximum possible resolution of approximately 2.5 wave numbers. If a δ_M of ±1 cm is considered, then

$$1 = \frac{2000\,(1)}{n_1}\,\theta_M^2, \quad \theta_M = 1.27\,n_1\ \text{degrees}.$$

This motion yields a resolution of approximately 1/4 wave number. The advantage of immersed interferometers follows from Snell's law

$$n_1 \sin\theta_1 = n_2 \sin\theta_2, \tag{4}$$

or for small angles $n_1\,\theta_1 = n_2\,\theta_2$. If the acceptance angle of the detector shown in Figure 7 is α, then for the immersed case $\theta_M = n\,\alpha$ and the solid angle increase is, still in the small angle approximation,

$$\Omega = \pi\,\theta_M^2 = \pi n^2\,\alpha^2$$

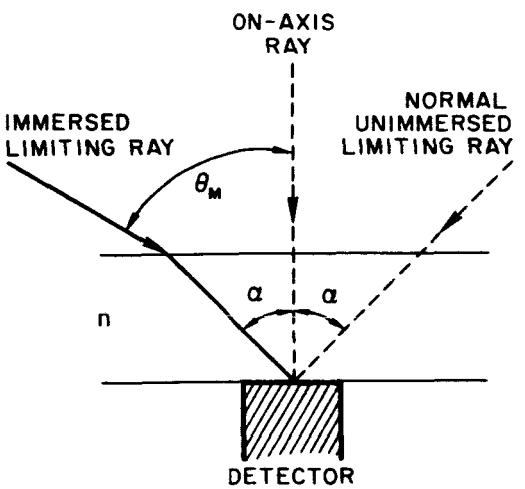

Figure 7—Detector with fixed acceptance angle.

For the proposed instrument however, the increase in cone half-angle is not proportional to n_1 but to $\sqrt{n_1}$. The reason for this is that in interferometer applications of immersion, the phase condition must also be considered. A gap of thickness δ, when filled with a material with index n, assumes an optical thickness δn. Equation (2) could be written as

$$\theta_M^2 = \frac{n}{\delta_M \sigma} = \frac{n^2}{\delta_M n \sigma}$$

which shows how the $\sqrt{n}$ dependence of θ_M arises.

C. Comments

1. Total Internal Reflection

When an electromagnetic wave crosses from one medium into an optically less dense medium, Equation (4) shows that if $\sin \theta_1 = n_2/n_1$ then $\theta_2 = \pi/2$ and no light enters the second medium.

This phenomenon can take place in the proposed instrument at the surface indicated by ℓ in Fig. 1, and redrawn in Fig. 8, the angles being related by:

$$\sin \theta_M = n_1 \sin \theta_1$$

$$n_1 \sin\left(\frac{\pi}{4} + \theta_1\right) = n_0 \sin \theta_0 = \frac{n_1}{\sqrt{2}}(\sin \theta_1 + \cos \theta_1)$$

we are concerned with the case when $\theta_0 = \pi/2$ or

$$\frac{n_0}{n_1}\sqrt{2} = \sin \theta_M + \left[1 - \frac{\sin^2 \theta_M}{n_1^2}\right]^{1/2}$$

If we impose arbitrarily the condition that the maximum value of θ_1 which the instrument is to be capable of accepting be $5° = .09$ radians, then the demand on the indices of refraction becomes

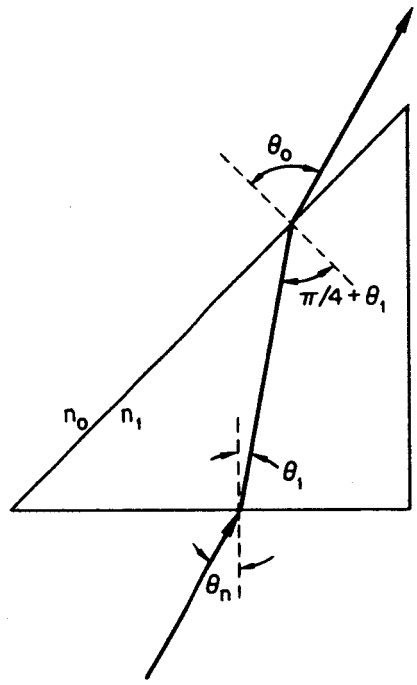

Figure 8–Total internal reflection occurs when $\theta_0 = \pi/2$

$$n_1 \sin\left(\frac{\pi}{4} + .09\right) = n_0 = \frac{n_1}{\sqrt{2}} (\sin .09 + \cos .09) = \frac{n_1}{\sqrt{2}} \left(.09 + 1 - \frac{.0081}{2}\right) = \frac{n_1}{\sqrt{2}} (1.1)$$

or

$$\frac{n_0}{n_i} = .78$$

If n_1 is 1.5 as for KBr then n_0 must be larger than 1.2.

Converting the cube into a parallel piped as in Figure 9 is an alternate method of eliminating total reflection. The angle of incidence, μ, at the critical interface is thus reduced. For KBr the limiting incidence angle is $\mu = \sin^{-1} (1/1.5) = 41.8°$ and for the same 5° internal off-axis limit we need $\nu = 36.8°$.

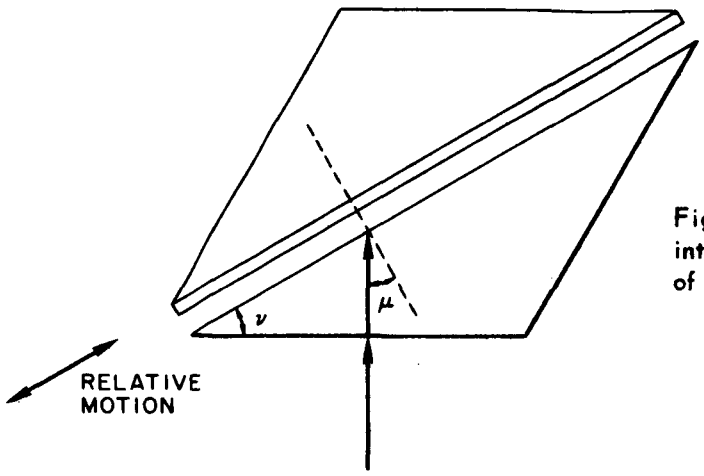

Figure 9–Configuration for avoiding total internal reflection by decreasing the angle of incidence, μ.

2. Mirror Motion

It is desirable that the mirror motion be linear in time and that the gap thickness indicated by k in Figure 1 be smaller than several of the shortest wavelengths to be analyzed, and constant to within a fraction of this. A wavelength of 5 microns corresponds to 200 micro-inches.

Preliminary talks with mechanical engineers indicate that the state of the art allows achieving a relative motion with the use of mechanical bearings of up to an inch while maintaining a separation of 100 microinches with a tolerance of ±50 microinches. Figure 10 shows how play in the relative motion mechanism bearings could give rise to an uncertainty in the gap of amount ϵ, which then is reduced by a factor of $1/\sqrt{2}$ in the uncertainty in mirror position. Unfortunately it is multiplied by $\sqrt{2}$ in determining the effect of the gap.

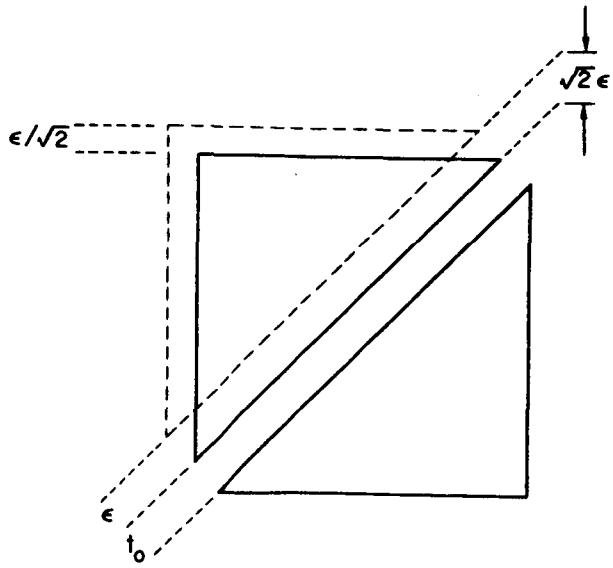

Figure 10–Effect of lateral displacement during mirror motion.

3. Aperture

A square aperture on the cube face where the input radiation is incident maximizes the energy acceptance for a fixed cube size and detector. As the limits of the relative motion increase the aperture necessarily becomes more of a rectangle, the side parallel to the motion becoming shorter.

It should be noted that aperture considerations are independent of field of view considerations, providing the aperture is small enough to allow the cube-face mirrors to transmit all the energy to the collecting optics. Thus a square aperture and a circular field of view are completely compatible.

III. THE INSTRUMENT FUNCTION

The method explained in Reference 2 yields the instrument function in terms of $h(\sigma, t)$, the energy input into the detector per unit wave number interval for unit spectral radiance, and other known or easily measured functions. Time is assumed linearly related to mirror position thru $\delta = v t$.

Reference 2 (bottom of page 5) gives the general expression for the instrument function

$$f(\sigma',\sigma) = {}_{t}F_{\omega} \left\{ Re \left[{}_{\omega'}F_{t}^{-1} \left\{ T(\omega') \; {}_{t'}F_{\omega'} \left\{ h(\sigma',t') D_{\tau}(t') \right\} \right\} D_{\tau}(t) \right] \right\} \quad (5)$$

Here the detector and the recorder are both activated between the times t_1 and t_2, with $t_1 = -\tau = t_2$, which are the symmetric limits on the rectangle function $D_{\tau}^{(t)}$. The operator taking the real part of the function of time t in the square brackets is actually not needed because the function is always real. This follows from the reality of $h(\sigma',t') D(t)$ and the fact that the electronic transfer function has the property $T(\omega) = T^{*}(-\omega)$. The relation between σ and ω will be shown to be

$$\omega = 4\pi\sigma v n_1 \left(1 - \frac{\theta_M^2}{4 n_1^2} \right) . \quad (6)$$

The units of the instrument function appear to need clarification. The defining equation

$$B_{measured}(\sigma) = \int_{-\infty}^{\infty} B_{real}(\sigma') \, f(\sigma',\sigma) \, d\sigma'$$

demands units of $1/cm^{-1}$ for the instrument function. Equation (9) however appears to have units of

$$\frac{A\pi\theta_M^2}{r} = \frac{cm^2 \text{ steradian}}{rad/sec} = \begin{bmatrix}\text{units of light} \\ \text{gathering power}\end{bmatrix} \text{sec},$$

since radians are dimensionless. That this is a trivial point to be taken care of by multiplication of $f(\sigma', \sigma)$ with a constant with units of $[cm^{-1}\, cm^2 \text{ steradian sec}]^{-1}$ is easily seen by inspection of the equation of reference 2 (page 5, 19th line) from which the instrument function (5) follows. The quantity on the right in that equation has units of watts sec and thus a constant with the units prescribed satisfies the conversion to units of spectral radiance.

The numerical valve of this constant depends upon the aperture area, the solid angle field of view, the gain level of the amplifiers, and perhaps other factors, such as length of mirror motion. In practice this aspect of the constant is not important because determination of an unknown spectrum is achieved thru calibration by comparing the computed spectrum from a known source with that from the unknown source.

A situation in which this constant actually becomes a function of wave number is conceivable. This could arise by demanding that the instrument function, including the not-necessarily-constant factor, give the same total power in the computed spectrum as existed in the real incident spectrum. The value of the number for wave number σ could be determined with quasi-monochromatic incident radiation of wave number σ and bandwidth well below the resolution of the instrument. Comparison of the power in the incident and computed spectra then yields the value of the number for that wave number. In practice this aspect of the factor is also not important because this is taken into account in the usual sensitivity or responsivity measurement.

A. Effect of Finite Mirror Motion and Solid Angle

The instrument function due to the non-infinite mirror motion and the non-zero solid angle of acceptance will now be found ignoring the contribution from the electronics, in which is included the equivalent circuit characterizing the detector response.

Assuming that $T(\omega)$ is constant, physically implies negligible electronic dispersion (phase shifting) and constant gain for all frequencies; equation 5 thus becomes, to within a constant,

$$f(\sigma', \sigma) = {}_tF_\omega \{h(\sigma', t)\, D_\tau(t)\} = \bar{h}(\sigma', \omega) \quad * \quad \bar{D}_\tau(\omega)$$

where * denotes convolution with respect to ω.

In this same approximation the interferogram becomes

$$I'(t) = D_\tau(t)\, I(t) = D_\tau(t) \int_0^\infty B(\sigma)\, h(\sigma, t)\, d\sigma.$$

Equation (2) may be written

$$h(\sigma', t) = A\pi\theta_M^2 \frac{\sin rt}{rt} \cos st \tag{7}$$

with

$$r = \frac{\pi\sigma' v \theta_M^2}{n_1}, \qquad s = 4\pi n_1 \sigma' v \left(1 - \frac{\theta_M^2}{4n_1^2}\right) \tag{8}$$

and Fourier transformed by convolution.

Thus,

$$\bar{h}(\sigma, \omega) = A\pi\, \theta_M^2 \int_{-\infty}^{\infty} \left[\frac{1}{r} \sqrt{\frac{\pi}{2}}\, D_r(\omega - \omega')\right] \left\{\sqrt{\frac{\pi}{2}} \left[\delta(\omega' - s) + \delta(\omega' + s)\right]\right\} d\omega'$$

$$= \frac{A\pi^2 \theta_M^2}{2r} \left[D_r(\omega - s) + D_r(\omega + s)\right]$$

where $D_r(x)$ is unity for x in the range $-r \le x \le r$, zero otherwise.

The instrument function then becomes, remembering that the exact relation between σ and ω is still to be made,

$$f(\sigma',\sigma) = \frac{A\pi\theta_M^2}{r}\sqrt{\frac{\pi}{2}}\int_{-\infty}^{\infty}[D_r(\omega'-s)+D_r(\omega'+s)]\ \frac{\sin(\omega-\omega')\tau}{(\omega-\omega')}\ d\omega' \qquad (9)$$

$$= \frac{A\,n_1}{\sigma'\,v}\sqrt{\frac{\pi}{2}}\ \Big\{Si([\omega-(s-r)]\tau) - Si([\omega-(s+r)]\tau + Si([\omega+(s-r)]\tau)$$

$$- Si([\omega+(s+r)]\tau\Big\} \qquad (10)$$

where

$$Si(x) = \int_0^x \frac{\sin y}{y}\,dy$$

is an odd function of its argument x, and r, s are related to σ' thru equation 8.

The last two terms are negligible for positive ω, and thus dropped because negative frequencies are not of interest. The quantity $r\tau$ is the maximum value of the argument of the natural apodizing function $\sin rt/rt$ in equation 7, and $2r\tau$ corresponds to the phase difference from the center to the edge of the detector when the mirror is at its maximum displacement. Since $1/v = \tau/\delta_M$ the v in the denominator causes the instrument function to increase linearly with integration time 2τ and to decrease inversely with maximum mirror displacement.

The first two terms in the curly brackets in equation 10 are shown in Figure 11. The horizontal axis variable is $\epsilon = \omega - s$. The parameter is $2r\tau$, the maximum phase difference across the detector face. It is related to the field of view thru

$$r\tau = \pi v' \delta_M \frac{\theta_M^2}{n_1}$$

since for the plot $\delta_M = .1$ cm and $\tau = 5$ sec. are held constant. The line with short dashes is $\sin \epsilon\tau/\epsilon\tau$ for comparison. Equation 9 shows that if the maximum value of $\epsilon\tau = r\tau << \pi$ then

$$\sin\frac{(\omega-\omega')\tau}{(\omega-\omega')}$$

is slowly varying under the narrow rectangle and may be taken outside the integral as

$$\frac{\sin(\omega - s)\tau}{(\omega - s)} .$$

The integral is then the area under the rectangle which decreases with solid angle decrease.

The instrument function is symmetric about $\epsilon = 0$. It is exactly this which justifies the relation of equation 6 between ω and σ. The resolution of the instrument for each parameter value can then be related to the width of the instrument function.

This set of curves are merely $\sin \epsilon\tau/\epsilon\tau$ curves convoluted with a rectangle function of variable width $2r\tau$. This can change both the amplitudes and the zero points of the $\sin \epsilon\tau/\epsilon\tau$ curve. If $2r\tau$ is an even multiple of π the largest amplitude central portion has half this number of pronounced peaks. If $2r\tau$ is an odd multiple of π the central portion is largely flat except for a maximum near each edge.

The effect on this family of curves of increasing δ_M by a factor u with velocity held constant and decreasing θ_M by $1/u^2$ is to merely cause the horizontal scale of Figure 11 to expand outward while the curves do not expand with the scale but remain the same. Thus the instrument function is narrowed. The parameter value of each curve then decreases by a factor of $1/u$. Increasing δ_M by a factor of u while holding both v and θ_M constant results generally in a squaring-up of each curve and a broadening approximately proportional to u, each parameter also increasing by the same amount. Intermediate between these two variations is the case where δ_M is increased by u and θ_M decreased by $\sqrt{1/u}$ with v held constant. Then each parameter value remains the same and each curve merely tends to become more square.

Figure 11 is essentially a comparison of total signal level for each field of view, or equivalently for each detector area. To compare signal-to-noise ratios each curve should be divided by a factor proportional to $\sqrt{r}$ or θ_M, and to compare signal per unit solid angle or per unit detector area each curve should be divided by a factor proportional to r or θ_M^2.

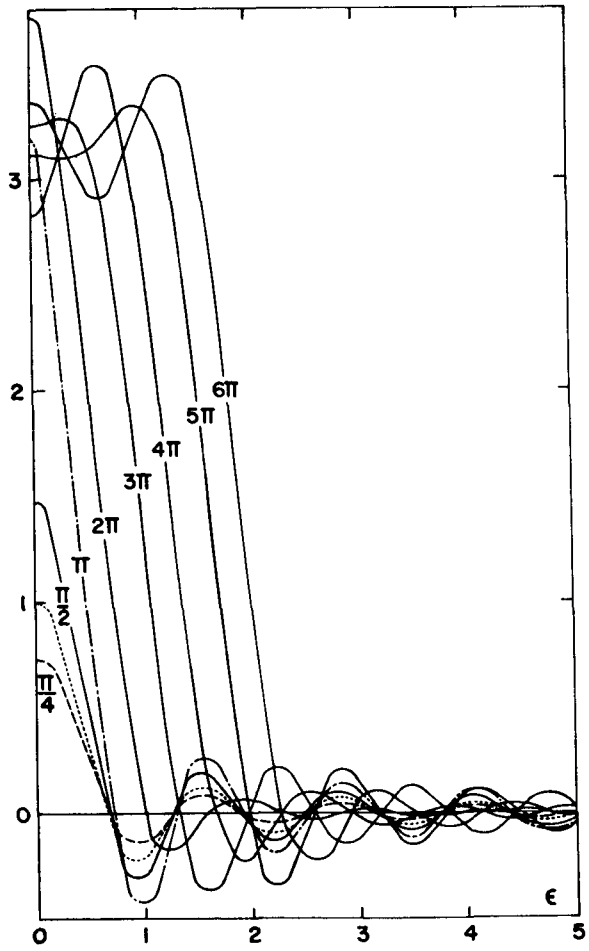

Figure 11–Plot of first 2 terms in curly brackets of equation 10, Si $[(\epsilon + r)\tau]$ – Si $[(\epsilon - r)\tau]$, with $\tau = 5$ sec and $\delta_M = .1$ cm. The parameter $2r\tau$ is the phased difference across the detector face with the mirror at its maximum displacement, and is proportional to the field of view. The short-dashed line is sin $\epsilon\tau / \epsilon\tau$ for comparison.

B. Resolution

The sin $\epsilon\tau/\epsilon\tau$ curve in Figure 11 has its first zero value at $\epsilon\tau = \pi$ or $\epsilon = .628$. The corresponding wave number interval $\Delta\sigma$ is found by the following. The definitions

$$\omega \equiv s + \epsilon \qquad s \equiv 4\pi n_1 v \sigma' \left(1 - \frac{\theta_M^2}{4n_1^2}\right)$$

lead naturally to

$$\omega = 4\pi n_1 v \left(1 - \frac{\theta_M^2}{4n_1^2}\right) (\sigma' + \Delta\sigma)$$

so that, neglecting θ^2 in comparison to unity,

$$\Delta\sigma = \frac{\epsilon}{4\pi n_1 v} = \frac{.628}{4\pi n_1 \frac{1}{50}} = \frac{2.5}{n_1} \text{ cm}^{-1} .$$

Thus the width of the central peak of the instrument function for the 3 smallest parameter values is 5 wave numbers for unity index of refraction, and the uncertainty for resolution considerations may of course be taken to be somewhat less than this. It is interesting to note that this uncertainty decreases with increasing index of refraction. This is to be expected because for a given mirror motion the optical path difference increases linearly with index of refraction.

There are two useful interpretations of Figure 11; for each the mirror velocity and maximum displacement have the same fixed values.

The first considers quasi-monochromatic input of fixed wave number. The set of curves then represents the computed spectra, the parameter now being proportional to the field of view, or detector size. Obviously the detector size corresponding to the parameter value π yields the highest amplitude curve with still the optimum resolution. The smaller detector areas yield smaller amplitude curves but with approximately the same resolution. The numerical factor mentioned before could be used to yield equally good results then with a smaller area detector. This is equivalent to a change in gain level of the electronics and leads to the usual noise considerations, the results usually being to use the detector corresponding to π, since the input radiation level is usually not overly strong.

The second interpretation considers a fixed detector size or solid angle and the parameter then is proportional to the wave number of different quasi-monochromatic inputs. This is of importance when analyzing broadband radiation. In this case the graph is not complete in that it does not show the effect of the wave number in the denominator of the expression (10) for the instrument function. Suppose the ratio of maximum to minimum wave number in the spectrum to be analyzed is 4. Figure 11 then shows that if we make the detector size such that the curve with parameter π corresponds to the maximum wave number, then the $\pi/4$ curve corresponds to the minimum wave number, except that this low amplitude curve must be multiplied by 4. Likewise the $\pi/2$ curve should be multiplied by 2, and would correspond to the instrument function of the central wave number. Thus the uncertainties pertinent to resolution are approximately the same for all wave numbers, and correspond to the optimum resolution for the detector size and mirror displacement.

If the curves were multiplied by the appropriate factors and replotted they would not quite overlap, the smaller parameter curves still having slightly smaller amplitude. To within the accuracy of the graphical method used to obtain the curves it is not a bad approximation to say that the instrument function is stationary or that $f(\sigma', \sigma) = f(\sigma' - \sigma)$. This holds however only while the maximum wave number corresponds to the curve with parameter equal to or less than π. If higher accuracy is desired then the more exact instrument function which is not stationary must be used.

IV. SUMMARY

The novel diagonal motion method of introducing a path difference and the use of two cube faces as mirrors constitutes a new configuration of the Michelson interferometer. There are two main advantages to the proposed configuration.

Because the configuration is effectively an immersed Michelson interferometer, the allowable field of view is increased linearly with the index of refraction of the solid material. This results in a higher signal level. Also more efficient use is made of the energy within the field of view because there are approximately 50% fewer reflecting interfaces, than in the conventional configuration each one of which causes part of the incident energy to be reflected back out of the instrument.

It seems quite possible to implement the relative half-cube motion with mechanical bearings to analyze wavelengths at least as short as 5 microns. Perhaps with new concepts in drive and support it would be possible to analyze still shorter wavelengths. A very smooth motion and constant thickness gap could perhaps be achieved by using the fluid with index of refraction n_0 as a fluid bearing.

V. ACKNOWLEDGMENT

I would like to thank Dr. R. Hanel for his guidance and helpful comments on many aspects of the broad area of interferometry. I am particularly indebted to him for his suggestion of the use of the parabolic surface and the alternate to the cube shape as discussed in Section II.C.1. I would also like to thank Michael L. Forman for his many valuable discussions of this field.

VI. REFERENCES

1. R. L. Hilliard, G. G. Shepherd, J.O.S.A. 56.3, March 1966, 11. 362-9, "Wide Angle Michelson Interferometer for Measuring Doppler Line Widths."

2. W. D. Johnson, III, "Theoretical Determination of the Instrument Function of the Michelson Interferometer Spectrometer," NASA/Goddard Space Flight Center, Internal Document X-622-66-325, July 1966.

3. Lawrence Mertz, Transformations in Optics, John Wiley & Sons, Inc., 1965.

4. Mme. Janine Connes, Revue d'Optique 40.2, 3, 4 and 5, 1961.